Accurate classification and selective observation of Rosen-Zener-Stückelberg resonances

Sheng-Chang Li [1,*] and Li-Bin Fu[2]

[1]*MOE Key Laboratory for Nonequilibrium Synthesis and Modulation of Condensed Matter,
Shaanxi Province Key Laboratory of Quantum Information and Quantum Optoelectronic Devices,
and School of Physics, Xi'an Jiaotong University, Xi'an 710049, China*
[2]*Graduate School, China Academy of Engineering Physics, Beijing 100193, China*

Rosen-Zener-Stückelberg (RZS) interferometry has provided an important tool for presenting and describing the quantum coherence in many systems, especially in ultracold atomic systems. In this paper we propose a Floquet matrix method to recognize the resonances induced by destructive RZS interference of a periodically driving two-level system with a $\sin^2$-type field. It is shown that the RZS resonances can be precisely distinguished into two classes: Regular resonance and accidental resonance. The former corresponds to the degenerate points in quasienergy spectrum and can be divided into integer resonance and half-integer resonance, while the latter is characterized by the eigenstate of a Floquet matrix with half of the components equaling to zero. We further discuss the possibility of experimentally observing these resonances. Particularly, it is found that a selective observation of different types of resonances can be realized in most cases by adjusting the time interval of periodic measurements.

I. INTRODUCTION

Quantum interference is one of the most fascinating and essential phenomena in quantum mechanics, which has been widely used in many fields such as quantum coherent control [1], precision measurement [2], and quantum metrology [3]. To demonstrate the physical characteristics of quantum interference, driven quantum two-level systems have been extensively studied because some of them can be solved analytically. Due to the rapid development of atomic cooling and control technology, the research on the coherent dynamics of two-level systems has set off a new upsurge in the field of ultracold atoms and molecules [4–9]. For the two-level model with a time-dependent energy difference, the most interesting signatures of quantum coherence are the interference patterns or the resonance structures that are formed by a distribution of the population probabilities in final state when a periodic driving field is imposed on the system. This famous scheme is often known as Landau-Zener-Stückelberg-Majorana (LZSM) interferometry [10–16], which can be observed in atomic and optical systems [17–19] or in superconducting qubit systems [20]. Recently, LZSM interferometry has been extended to nonlinear [21] and non-Hermitian [22] situations.

Another important interference scheme of two-level systems is Rosen-Zener (RZ) interferometry [23] based on the RZ tunneling process [24], which is characterized by a constant energy bias and a periodically time-varying coupling in contrast to the LZ interference scheme [15]. The RZ model was first proposed to investigate the spin-flip of two-level atoms interacting with a rotating magnetic field and used to explain the double Stern-Gerlach experiments [25]. The simple linear RZ

model [26] was then generalized to the nonlinear case [24] and has been used to study the formation of cold molecules [27]. Two RZ pulses can be used to build a Ramsey interferometer [28] with a two-component Bose-Einstein condensate (BEC) [29] or a double-well BEC in an optical cavity [30]. This type of interferometry has potential applications in calibrating the atomic parameters or allows nondestructive observations of atomic Ramsey fringes via the cavity transmission spectra. When applying a sequence of RZ pulses to double-well BEC, we constructed a new type of interference scheme, namely, Rosen-Zener-Stückelberg (RZS) interferometry [31], which can be realized by periodically changing the height or width of the barrier between two wells [32,33].

In this paper we develop a method based on Floquet theory to accurately identify the key information in RZS interference patterns without solving the Schrödinger equation. A similar approach called Floquet determinant method has been successfully used to characterize LSZM resonances [16]. For our quantum two-level RZS interferometry with a periodic $\sin^2$-type coupling field, the key information directly correspond to the points of destructive interference in the parameter space, also known as coherent destruction of tunneling [34,35], and for consistency we call them RZS resonances. We focus on classifying the resonances into different kinds and explore the possibility of their experimental observation. By establishing the relation between the parameter values of resonance points and the eigenvalues or eigenstates of the corresponding infinite Floquet matrices (FMs), we find that the FM approach can exactly give all RZS resonance positions so that we can better understand the nature of RZS interferences.

Compared with the results obtained from previous study on LZSM interferometry with a sin-type field [16], we have two main points. (i) By accurately diagonalizing the finite FMs, we can strictly divide all RZS resonances with

sin^2-type field into two categories, namely, regular resonances and accidental resonances. The regular resonances correspond to the degenerate points in quasienergy spectrum composed of the eigenvalues of FM, which can be further subdivided into the integer and half-integer resonances according to the relation between degenerate energy and driving frequency. In short, our two kinds of normal resonances are real resonances and our accidental resonances are insensitive to the phase of the driven field. However, in Ref. [16] both real and complex resonances were found, and they showed that the accidental resonances are sensitive to the phase of the field. (ii) More importantly, all types of our RZS resonances identified by FM method can be observed experimentally by periodically measuring the population probability in final state. In particular, in most parameter regions we can achieve a selective observation of different types of RZS resonances by adjusting the time interval of periodic measurements. Unfortunately, both the complex resonance and the accidental resonance mentioned in the literature [16] cannot be observed experimentally.

The rest of the paper is organized as follows. Section II contains the main results of the paper. We introduce RZS interferences and resonances, we present our analysis based on FM method, we discuss the relevant classes of RZS resonances, and we show how to observe different kinds of resonances. Section III summarizes the paper.

II. CLASSIFICATION AND OBSERVATION OF RZS RESONANCES

A. RZS resonances

The quantum two-level RZS interferometry scheme is characterized by the following time-dependent Hamiltonian [24,29]:

$$H(t) = \frac{\Delta}{2}\hat{\sigma}_z + \frac{V(t)}{2}\hat{\sigma}_x, \tag{1}$$

where $\hat{\sigma}_{x,z}$ represent Pauli matrices; $V(t+T) = V(t) = V_0 + A\sin^2(2\omega t)$ denotes a continuous RZ-pulse driving field with amplitude A, offset V_0, and frequency 2ω or period $T = \frac{\pi}{2\omega}$; and the constant Δ is the energy bias between the two states labeled by $|a\rangle$ and $|b\rangle$ with a and b being the population probabilities for the system to be in these states. A typical physical system described by this simple two-level model is a spin-$\frac{1}{2}$ particle in a static magnetic field with a continuous-pulse-magnetic field applied perpendicular to the static field [36]. Another physical system is two-component BEC without atomic interaction [29] or two-mode interaction-free ultra-cold atoms trapped in a double-well potential with a periodic modulation barrier [31]. For convenience, we write the time-dependent Schrödinger equation in matrix form ($\hbar = 1$)

$$i\frac{d}{dt}X(t) = H(t)X(t), \quad X(t) = \begin{pmatrix} a(t) & -b^*(t) \\ b(t) & a^*(t) \end{pmatrix}, \tag{2}$$

with normalization condition $|a|^2 + |b|^2 = 1$. Initially, the system is prepared in state $|a\rangle$, i.e., $a(0) = 1$ and $b(0) = 0$, then $P_b = |b|^2$ represents the transition probability to state $|b\rangle$, and is a function of t, A, ω, and Δ. The probability P_b after N
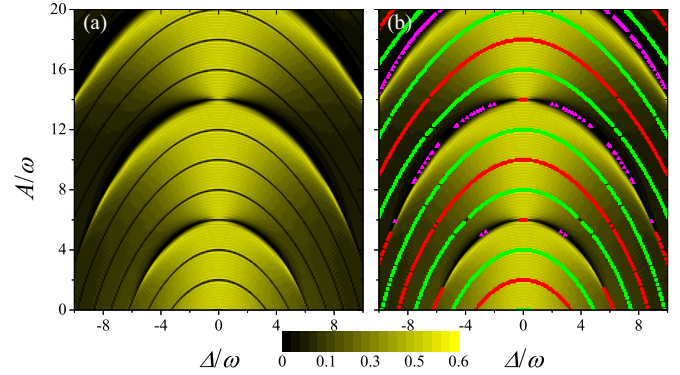

FIG. 1. (a) Periodic-averaged population probability $\bar{P}_b(n\tau)$ as a function of driving amplitude A and energy detuning Δ from numerical solution of Schrödinger equation with $V_0 = 5\omega$, $\tau = 4T$, and $n = 10$. (b) Red circles, green squares, and purple triangles mark zero-value degenerate eigenenergies, nonzero-value degenerate eigenenergies, and zero-value eigenstates of FM, respectively.

RZ pulses is [14,16]

$$P_b(NT) = \frac{\sin^2(N\cos^{-1}\{\text{Re}[a(T)]\})}{1 - \text{Re}[a(T)]^2}|b(T)|^2. \tag{3}$$

Consider in experiments the final probability $P_b(t)$ is averaged over many pulses, we mainly focus on the quantity $\bar{P}_b(n\tau) = \frac{1}{n}\sum_{m=1}^{n} P_b(m\tau)$ for n measurements with periodic interval τ being integer multiples of T. It must be mentioned that the average operation only narrows the interference fringes but does not change the density and position of fringes. In this paper we choose $n = 10$, $\tau = T$, $2T$, and $4T$, to show the resonances induced by destructive RZS interference [31]. Here we label the position where the periodic-averaged probability $\bar{P}_b(n\tau)$ vanishes in the parameter space spanned by (A, ω, V_0, Δ) as a RZS resonance. RZS interference patterns are formed by the collections of such resonances. Figure 1(a) illustrate the interference pattern for $n = 10$, $\tau = 4T$, and $V_0 = 5\omega$ as an example. For $\Delta = 0$, the analytically periodic solution of Eq. (2) reads

$$P_b(\tau) = \sin^2\theta(\tau), \quad \theta(\tau) = \frac{1}{4}(A + 2V_0)\tau. \tag{4}$$

Thus, the resonance positions shown in Fig. 1(a) are determined by $\theta(4T) = \frac{(A+10\omega)\pi}{2\omega} = k\pi$ (with integer k), i.e., $A = (2k - 10)\omega$ with $k \geqslant 5$, which are in good agreement with the numerical results obtained from solving Schrödinger equation.

B. Floquet matrix method

According to Floquet's theorem, the solution of Eq. (2) can be expressed as $X(t) = \Phi(t)\exp(-iEt)$, where $\Phi(t)$ is a matrix of periodic functions of t and E is a constant diagonal matrix with diagonal elements $\pm\epsilon$ called quasienergy. Then the time-evolution operator can be written as follows:

$$U(t) = \Phi(t)e^{-iEt}\Phi(0), \quad \Phi = \begin{pmatrix} \phi_{aa} & -\phi_{ba}^* \\ \phi_{ba} & \phi_{aa}^* \end{pmatrix}, \tag{5}$$

where $\phi_{aa}(t+T) = \phi_{aa}(t)$ and $\phi_{ba}(t+T) = \phi_{ba}(t)$ are periodic functions with $|\phi_{aa}|^2 + |\phi_{ba}|^2 = 1$. Combing Eqs. (2) and (5) at $t = \tau$ gives the transition probability after several

RZ pulses

$$P_b(\tau) = 4|\phi_{aa}(0)|^2|\phi_{ba}(0)|^2 \sin^2(\epsilon\tau). \quad (6)$$

This equation implies that the transition probability $P_b(\tau)$ [and hence $\bar{P}_b(n\tau)$] is equal to zero only when $\epsilon\tau = k\pi$ corresponding to periodic evolution, or when $|\phi_{aa}(0)||\phi_{ba}(0)| = 0$ corresponding to nonperiodic motion in general [16]. As a result, we can divide RZS resonances into two natural classes: The regular resonances determined by $\epsilon\tau = k\pi$ and the accidental resonances associated with $|\phi_{aa}(0)||\phi_{ba}(0)| = 0$. It is worth noting that, in rare cases, both two conditions are satisfied, the resonances will be referred to as regular resonances.

We emphasize that it is necessary to classify RZS resonances into different types because in many cases we can selectively observe different resonances in experiments. The regular resonances reflect the global properties of the system and only depend on the quasienergy spectrum. The accidental resonances are different, they are closely related to the selection of initial conditions and thus they only display the local characteristics of the system [16]. Amazingly, we find that, for the periodic field we adopted, the accidental resonances are not sensitive to the phase of the field, and therefore they can be clearly observed in experiments. Moreover, we show that the regular resonances are not weakened after averaging over many periodic measurements and we can narrow the resonance dips by increasing the number of periodic measurements to enhance the observation accuracy. These results are different from those for LZSM interferometry with a sin-type field [16].

There are two advantages of using the Floquet method to study resonances: (i) we do not need to solve the time-dependent Schrödinger equation; and (ii) we can obtain the exact locations of the resonances. The fact that the regular resonances are determined solely by the special quasienergy values allows us to accurately identify RZS resonance positions by Floquet quasienergy spectra. To this end, we expand the periodic functions $\phi_{aa}(t)$ and $\phi_{ba}(t)$ in Fourier series, i.e., $\phi_{aa}(t) = \sum_{n_F} x_{aa}^{n_F} \exp(in_F\omega t)$ and $\phi_{ba}(t) = \sum_{n_F} x_{ba}^{n_F} \exp(in_F\omega t)$. Then the matrix elements of the solution $X(t)$ can be expressed as follows:

$$a(t) = \sum_{n_F=-\infty}^{+\infty} x_{aa}^{n_F} e^{in_F\omega t} e^{-i\epsilon t}, \quad (7)$$

$$b(t) = \sum_{n_F=-\infty}^{+\infty} x_{ba}^{n_F} e^{in_F\omega t} e^{i\epsilon t}. \quad (8)$$

For consistency we have used subscripts a and b to denote the matrix elements. Similarly, we expand the matrix elements of Hamiltonian (1) in Fourier series as

$$(H)_{ab} = \sum_{n_F} h_{ab}^{n_F} e^{in_F\omega t}. \quad (9)$$

It must be mentioned that, when we expand the above quantities in Fourier series we do not use the frequency of the periodically driving field (i.e., 2ω), but half of it (i.e., ω). This operation is crucial to the selective observation of different types of RZS resonances discussed later and differs from that in Ref. [16]. Substituting the expansions (7), (8), and (9) back

into Schrödinger equation (2), we can obtain a set of recursion relations between the Fourier coefficients $x_{ab}^{n_F}$, which are

$$\sum_{c,m_F}(M_F)_{an_F,cm_F}x_{ca}^{m_F} = \epsilon x_{aa}^{n_F}, \quad (10)$$

$$\sum_{c,m_F}(M_F)_{an_F,cm_F}x_{cb}^{m_F} = -\epsilon x_{ab}^{n_F}, \quad (11)$$

with $c = a, b$, and $m_F = -\infty, \ldots, +\infty$; where M_F is an infinite Hermitian matrix with elements being

$$(M_F)_{an_F,bm_F} = h_{ab}^{n_F-m_F} + n_F\omega\delta_{ab}\delta_{n_Fm_F}. \quad (12)$$

C. Accurate classification

For convenience, we order the matrix elements so that a runs over two states labeled by a and b before each change in Fourier index n_F. We refer to M_F as a FM associated with the quantum Hamiltonian (1). Finally, we can derive a matrix eigenvalue equation

$$M_F X_F = \Lambda X_F, \quad (13)$$

where $X_F = (\ldots, x_{aa}^{-1}, x_{ba}^{-1}, x_{aa}^0, x_{ba}^0, x_{aa}^{+1}, x_{ba}^{+1}, \ldots)^T$ is a column vector composed of Fourier coefficients; Λ is a diagonal matrix with the diagonal elements cyclically arranged by $\pm\epsilon$. For given periodic pulse field $V(t)$ and energy bias Δ, we can construct M_F and obtain the corresponding Floquet quasienergy spectrum by solving Eq. (13). The degenerate (i.e., crossing) points in the quasienergy spectrum correspond to the locations of RZS resonances in the interference patterns. We emphasize that all eigenvalues of M_F are real for our model and thus they are physical solutions. The RZS resonances identified by the crossing points of quasienergy levels are all regular resonances, which are easy to observe experimentally. For example, in Fig. 1(b) we plot the points where the eigenvalues of FM are degenerate together with the interference patterns for $V_0 = 5\omega$. We find that these points can be divided into two categories: The intersections appear at the positions with quasienergy being $l\omega$ (marked by red circles) and the intersections occur at the positions with quasienergy being $(l \pm \frac{1}{2})\omega$ (denoted by green squares). They constitute two types of regular resonances, namely, integer resonances and half-integer resonances. It is worth noting that both of these two types of regular resonances are real resonances due to real quasienergy values and there is not a complex resonance with a complex quasienergy value as demonstrated in Ref. [16].

In addition to the integer and half-integer resonances mentioned above, there are some RZS resonances that are not recognized by the degenerate points in Floquet quasienergy spectra. Fortunately, these resonances can be captured by analyzing the eigenstates of FM. According to the criterion for accidental resonances obtained from Eq. (6), we can rewritten the condition as $\sum_{n_F} x_{aa}^{n_F} \sum_{m_F} x_{ba}^{m_F} = 0$, which means that half of the components of one eigenstate of FM are equal to zero. In Fig. 1(b) we plot the points by purple triangles where the condition $|\sum_{n_F} x_{aa}^{n_F}| \leqslant 10^{-2}$ or $|\sum_{m_F} x_{ba}^{m_F}| \leqslant 10^{-2}$ is satisfied due to the finite dimensional FM in actual computation. We find that the convergence with respect to the cutoff dimension of FM is very rapid and the dimension of the matrix we
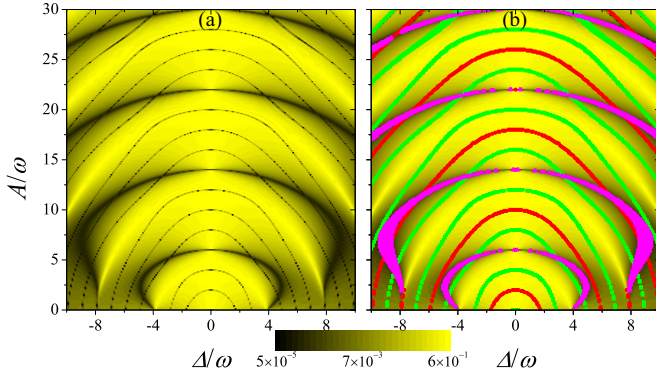
FIG. 2. (a) Periodic-averaged population probability $\bar{P}_b(n\tau)$ as a function of driving amplitude A and energy detuning Δ from the numerical solution of the Schrödinger equation with $V_0 = \omega$, $\tau = 4T$, and $n = 10$. (b) Red circles, green squares, and purple triangles mark zero-value degenerate eigenenergies, nonzero-value degenerate eigenenergies, and zero-value eigenstates of FM, respectively.

FIG. 3. (a) Periodic-averaged population probability $\bar{P}_b(n\tau)$ as a function of driving amplitude A from a numerical solution of the Schrödinger equation for different τ with $n = 10$, $\Delta = 0$, and $V_0 = \omega$. (b) Partial eigenvalues of FM as a function of A. Vertical broken red lines and dash-dotted black lines mark zero-value degenerate and nonzero-value degenerate positions, respectively.

adopted is greater than or equal to 4 times of the maximum value of driving amplitude A.

To see the influence of the offset V_0 on the classification of RZS resonances, we also plot the interference patterns and the resonance positions identified by the above FM method with $V_0 = \omega$ in Fig. 2. When $\Delta = 0$, it is found that the integer (red circles) and half-integer (green squares) resonances always alternately occur in parameter A domain. When $\Delta \neq 0$, the accidental resonances emerge. It is easy to see that the accidental resonance are always separate from the regular resonances for large V_0 [see Fig. 1(b)]; whereas, for small V_0 [see Fig. 2(b)], the accidental resonances can overlap with the regular resonances (integer or half-integer) in very few cases.

D. Selective observation

Now we elaborate on how to carry out effective experimental observation on the above various RZS resonance structures. In order to avoid the reduction of the number of resonance dips caused by the periodic averaging operation, we do not take the final population probability $P_b(t) = |b(t)|^2$ as the observable, but view the periodic-averaged population probability $\bar{P}_b = \frac{1}{n}\sum_{m=1}^{n} P_b(m\tau)$ as the observation quantity, which can be obtained by averaging the results of n measurements $P_b(m\tau)$ that recorded after every j RZ pulses (i.e., $\tau = jT$ with T being pulse duration). We have confirmed that the individual resonances become sharper as the number of measurements n is increased. Furthermore, we have found that all RZS resonances given by $\bar{P}_b$ do not become less visible or disappear as the number of measurements increases and thus they are robust in the limit of large n.

In Fig. 3(a) we plot the resonances as a function of A/ω for $\tau = T$, $2T$, and $4T$ with $n = 10$, $\Delta = 0$, and $V_0 = \omega$. In this case, the resonance positions are determined by the analytical condition: $\sin[\frac{1}{4}(A + 2\omega)\tau] = 0$, which are exactly the points captured by the Floquet quasienergy spectrum as demonstrated in Fig. 3(b). Comparing Figs. 3(a) and 3(b) we find that in this case there are only regular resonances and no accidental resonance. If we take $\tau = T$ for measurement, only partial integer resonances can be observed. If we set $\tau = 2T$,
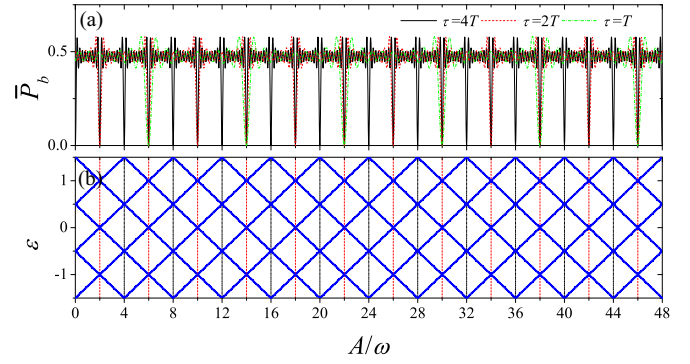
all integer resonances can be observed. If $\tau = 4T$, all regular resonances including integer and half-integer resonances can be observed. In the general case, $\Delta \neq 0$. We take $\Delta = \sqrt{2}\omega$ as an example and plot the resonances as a function of A/ω also for $\tau = T$, $2T$, and $4T$ with $n = 10$ and $V_0 = \omega$ in Fig. 4(a) together with the corresponding Floquet quasienergy spectrum illustrated in Fig. 4(b). Obviously the degenerate points of the quasienergy levels in the spectrum can recognize only part of RZS resonances (i.e., regular resonances) in Fig. 4(a). The rest of RZS resonances are of course accidental resonances, and their positions are exactly consistent with those [marked by the purple triangles in Fig. 4(a)] obtained by using the criterion $|\sum_{n_F} x_{aa}^{n_F}| \leqslant 10^{-2}$ or $|\sum_{m_F} x_{ba}^{m_F}| \leqslant 10^{-2}$ given by the eigenstates of FM. Particularly if we take $\tau = T$ for measurement, only accidental resonances can be observed. If we set $\tau = 2T$, both accidental and integer resonances can be observed. If $\tau = 4T$, both accidental and regular resonances can be observed. These results suggest that we can make selective observations of the different types of
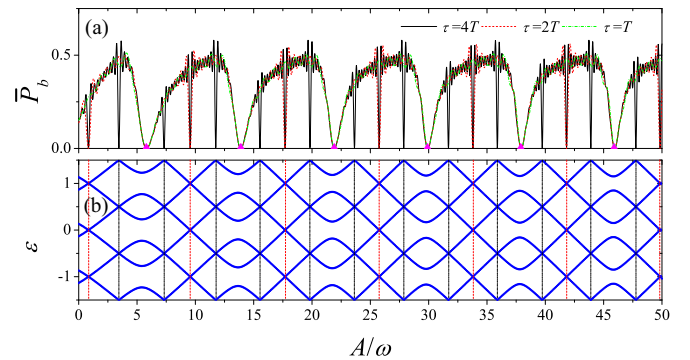

FIG. 4. (a) Periodic-averaged population probability $\bar{P}_b(n\tau)$ as a function of A from a numerical solution of the Schrödinger equation for different τ with $n = 10$, $\Delta = \sqrt{2}\omega$, and $V_0 = \omega$. Purple triangles denote the points where exist zero-value eigenvectors of FM. (b) Partial eigenvalues of FM. Vertical broken red lines and dash-dotted black lines mark zero-value degenerate and nonzero-value degenerate positions, respectively.
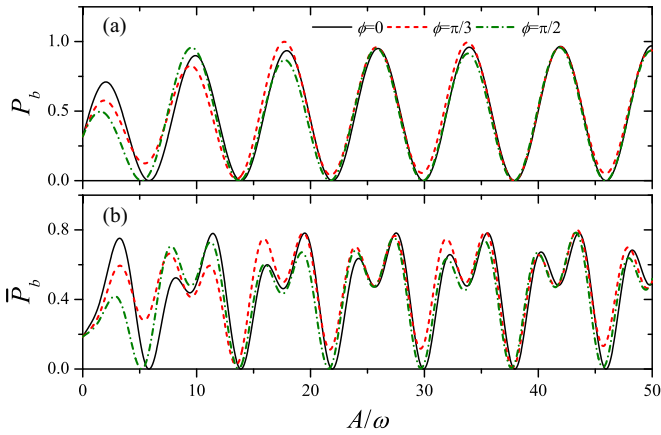
FIG. 5. (a) Final population probability $P_b(T)$ as a function of A for different field phases ϕ. (b) Periodic-averaged population probability $\bar{P}_b(n\tau)$ as a function of A for different ϕ with $n = 2$ and $\tau = T$. The minimum values of each line correspond to the positions of accidental resonances. The parameters are $\Delta = \sqrt{2}\omega$ and $V_0 = \omega$.

RZS resonances by adjusting the time interval τ between measurements.

Finally, we discuss the effect of the phase of the periodically driving field on the accidental resonances. To this end, we rewrite the field as $V(t) = V_0 + A \sin^2(2\omega t + \phi)$, with ϕ being the initial phase of the field. According to the above proposed rule of selective observation, accidental RZS resonance occurs only in the measurements where $\Delta \neq 0$ and $\tau = T$. This means that the accidental resonance can also be observed simply by measuring the final occupancy probability P_b at $t = T$. For comparison, in Fig. 5 we plot the results of both the final occupation probability [see Fig. 5(a)] and the periodic-averaged occupation probability [see Fig. 5(b)] for different initial phases. Obviously the minimum values of

occupation probabilities correspond to the positions of accidental resonances. In contrast to the results that the accidental resonance is sensitive to the phase of the field and cannot be observed experimentally [16], it is easy to see that in our case the accidental resonances are not sensitive to the initial phase of the field. This is why they can be observed in other periodic-averaged measurements [e.g., $\tau = 2T$ or $4T$, see Fig. 4(a)].

III. CONCLUSION

To summarize, we have demonstrated a general framework based on Floquet matrix for exactly classifying Rosen-Zener-Stückelberg (RZS) resonances into two main categories, respectively, characterized by the degenerate points in Floquet quasienergy spectrum and the eigenstate of Floquet matrix with half of the components being zero. The different types of RZS resonances identified by our method do not require solving the Schrödinger equation and can be selectively observed experimentally in most parameter regimes. The main difference between our Floquet matrix approach and the others is that we expand the physical quantities in Fourier series with half of the frequency of the driving field instead of itself. This operation rescales the Floquet matrix and changes the structure of the matrix, which provides the basis for realizing the selective observation of RZS resonances via periodic measurements. It is worth mentioning that the Floquet matrix method used in this paper can be generalized to other types of resonances including nonlinear cases.

[1] B. P. Anderson and M. A. Kasevich, Science **282**, 1686 (1998).

[2] A. Peters, K. Y. Chung, B. Young, J. Hensley, and S. Chu, Philos. Trans. R. Soc. London Ser. A **355**, 2223 (1997).

[3] L. Pezzè, A. Smerzi, M. K. Oberthaler, R. Schmied, and P. Treutlein, Rev. Mod. Phys. **90**, 035005 (2018).

[4] A. Smerzi, S. Fantoni, S. Giovanazzi, and S. R. Shenoy, Phys. Rev. Lett. **79**, 4950 (1997).

[5] S. Raghavan, A. Smerzi, S. Fantoni, and S. R. Shenoy, Phys. Rev. A **59**, 620 (1999).

[6] A. J. Leggett, Rev. Mod. Phys. **73**, 307 (2001).

[7] E. A. Donley, N. R. Claussen, S. T. Thompson, and C. E. Wieman, Nature (London) **417**, 529 (2002).

[8] T. Köhler, K. Góral, and P. S. Julienne, Rev. Mod. Phys. **78**, 1311 (2006).

[9] J. Liu, S. C. Li, L. B. Fu, and D. F. Ye, *Nonlinear Adiabatic Evolution of Quantum Systems: Geometric Phase and Virtual Magnetic Monopole* (Springer, Singapore, 2018).

[10] L. D. Landau, Phys. Z. Sowjetunion **2**, 46 (1932).

[11] C. Zener, Proc. R. Soc. London Ser. A **137**, 696 (1932).

[12] E. C. G. Stückelberg, Helv. Phys. Acta **5**, 369 (1932).

[13] E. Majorana, Nuovo Cimento **9**, 43 (1932).

[14] S. Shevchenko, S. Ashhab, and F. Nori, Phys. Rep. **492**, 1 (2010).

[15] E. Barnes, Phys. Rev. A **88**, 013818 (2013).

[16] S. Ganeshan, E. Barnes, and S. Das Sarma, Phys. Rev. Lett. **111**, 130405 (2013).

[17] M. C. Baruch and T. F. Gallagher, Phys. Rev. Lett. **68**, 3515 (1992).

[18] S. Yoakum, L. Sirko, and P. M. Koch, Phys. Rev. Lett. **69**, 1919 (1992).

[19] J. Q. You and F. Nori, Nature (London) **474**, 589 (2011).

[20] X. Tan, D. W. Zhang, Z. Zhang, Y. Yu, S. Han, and S. L. Zhu, Phys. Rev. Lett. **112**, 027001 (2014).

[21] S. C. Li, L. B. Fu, and J. Liu, Phys. Rev. A **98**, 013601 (2018).

[22] X. Shen, F. Wang, Z. Li, and Z. Wu, Phys. Rev. A **100**, 062514 (2019).

[23] L. B. Fu, D. F. Ye, C. Lee, W. Zhang, and J. Liu, Phys. Rev. A **80**, 013619 (2009).

[24] D. F. Ye, L. B. Fu, and J. Liu, Phys. Rev. A **77**, 013402 (2008).

[25] N. Rosen and C. Zener, Phys. Rev. **40**, 502 (1932).

[26] R. T. Robiscoe, Phys. Rev. A **17**, 247 (1978).

[27] A. Ishkhanyan, R. Sokhoyan, B. B. Joulakian, and K.-A. Suominen, Opt. Commun. **282**, 218 (2009).

[28] N. F. Ramsey, Phys. Rev. **78**, 695 (1950).

[29] S. C. Li, L. B. Fu, W. S. Duan, and J. Liu, Phys. Rev. A **78**, 063621 (2008).

[30] S. C. Li, F. Q. Dou, and L. B. Fu, Opt. Lett. **42**, 3952 (2017).

[31] S. C. Li and L. B. Fu, Phys. Rev. A **101**, 023618 (2020).

[32] T. Berrada, S. van Frank, R. Bücker, T. Schumm, J.-F. Schaff, and J. Schmiedmayer, Nat. Commun. **4**, 2077 (2013).

[33] T. Berrada, S. van Frank, R. Bücker, T. Schumm, J.-F. Schaff, J. Schmiedmayer, B. Julía-Díaz, and A. Polls, Phys. Rev. A **93**, 063620 (2016).

[34] J. Stehlik, Y. Dovzhenko, J. R. Petta, J. R. Johansson, F. Nori, H. Lu, and A. C. Gossard, Phys. Rev. B **86**, 121303(R) (2012).

[35] F. Grossmann, T. Dittrich, P. Jung, and P. Hänggi, Phys. Rev. Lett. **67**, 516 (1991).

[36] J. H. Shirley, Phys. Rev. **138**, B979 (1965).